Spontaneous symmetry breaking in a nonlinear double-well structure

Thawatchai Mayteevarunyoo,[1,2] Boris A. Malomed,[2] and Guangjiong Dong[3]

[1]*Department of Telecommunication Engineering, Mahanakorn University of Technology, Bangkok 10530, Thailand*
[2]*Department of Physical Electronics, School of Electrical Engineering, Faculty of Engineering,*
Tel Aviv University, Tel Aviv 69978, Israel
[3]*State Key Laboratory of Precision Spectroscopy and Physics Department, East China Normal University, Shanghai, China*

We propose a model of a nonlinear double-well potential (NDWP), alias a double-well pseudopotential, with the objective to study an alternative implementation of the spontaneous symmetry breaking (SSB) in Bose-Einstein condensates (BECs) and optical media, under the action of a potential with two symmetric minima. In the limit case when the NDWP structure is induced by the local nonlinearity coefficient represented by a set of two delta functions, a fully analytical solution is obtained for symmetric, antisymmetric, and asymmetric states. In this solvable model, the SSB bifurcation has a fully subcritical character. Numerical analysis, based on both direct simulations and computation of stability eigenvalues, demonstrates that, while the symmetric states are stable up to the SSB bifurcation point, both symmetric and emerging asymmetric states, as well as all antisymmetric ones, are unstable in the model with the delta functions. In the general model with a finite width of the nonlinear-potential wells, the asymmetric states quickly become stable, simultaneously with the switch of the SSB bifurcation from the subcritical to supercritical type. Antisymmetric solutions may also get stabilized in the NDWP structure of the general type, which gives rise to a bistability between them and asymmetric states. The symmetric states require a finite norm for their existence, an explanation to which is given. A full diagram for the existence and stability of the trapped states in the model is produced. Experimental observation of the predicted effects should be possible in BEC formed by several hundred atoms.

I. INTRODUCTION

The one-dimensional (1D) Schrödinger equation including a symmetric potential structure produces single-particle wave functions of a definite parity, even or odd, with the ground state always corresponding to an even function without zeros. However, a spatially symmetric Hamiltonian of an interacting many-particle system can give rise to asymmetric states, which may be considered as a spontaneous-symmetry-breaking (SSB) effect. At the classical level, the SSB occurs in optics, as a result of the interplay between the nonlinearity and waveguiding structures, when the strong nonlinearity partly suppresses the linear coupling between parallel guiding cores. In particular, it was shown that a stable trapped mode may be asymmetric in a channel waveguide embedded in the self-focusing Kerr medium [1]. The onset of a sharp symmetry-breaking instability in a double-hump two-component spatial optical soliton was demonstrated experimentally in a planar nonlinear waveguide [2].

A natural setting in which SSB phenomena may arise in the context of nonlinear optics and Bose-Einstein condensation (BEC) is provided by double-well potentials (DWPs). In the experiment, an effective optical DWP was created by a specially designed illumination pattern applied, in the ordinary polarization, to a photorefractive crystal (the SSB was observed in a beam with extraordinary polarization, shone through this structure) [3]. It was also proposed to realize similar effective potentials in coupled nonlinear microcavities [4], and in a structured core of an optical fiber [5]. A specific variety of the optical SSB was studied in a model of two parallel-coupled antiwaveguides with the self-focusing nonlinearity, which corresponds to an effective double-barrier potential, rather than DWP [6].

Well-known dual-core optical fibers [7], which may serve as a basis for the power-controlled all-optical switching, if the Kerr nonlinearity is taken into regard [8], may also be considered as DWP structures, with the difference that the tunneling between two potential wells is replaced by the linear coupling between the cores. In addition to the SSB of continuous-wave states [9], the formation of asymmetric solitons in dual-core fibers was studied in detail theoretically [10]. Similar analysis of the SSB for soliton modes was performed in models of dual-core fiber Bragg gratings with the Kerr nonlinearity [11], and coupled waveguides with the quadratic [12] and cubic-quintic [13] nonlinear terms, including a system of linearly coupled complex Ginzburg-Landau equations of the cubic-quintic type [14]. In Refs. [15–17], the analysis of the SSB was extended to three-core linearly coupled triangular configurations—for optical fibers, Bragg gratings, and complex Ginzburg-Landau equations, respectively.

The concept of SSB also plays an important role in understanding experimental phenomena in BEC, because, if interactions between atoms are strong enough, the ground state of the condensate may not follow the symmetry of the trapping potential [18]. In particular, manifestations of SSB were observed in a quenched ferromagnetic state of a spinor (three-component) condensate [19]. In the single-component BEC, a natural setting for the realization of SSB may again be provided by DWP configurations. An effectively one-dimensional DWP structure was realized experimentally in Ref. [20]. Loading a condensate of ^{87}Rb atoms with the repulsive interaction between them into this structure made it possible to observe Josephson oscillations for a small number of atoms, and the macroscopic quantum self-trapping

featuring an imbalance between populations of the two wells, for a larger number. Parallel to the experimental work, numerous theoretical studies of matter-wave DWP settings have been performed for the cases of both repulsion and attraction between atoms. These studies addressed problems such as finite-mode reductions [21] (including two-component mixtures [22]), obtaining analytical results for specific shapes of the potential [23], quantum effects [24], and some others. Recently investigated tunneling between vortex and antivortex states in BEC trapped in a two-dimensional (2D) anisotropic potential [25] belongs to this category too.

Theoretical analysis was also performed for 2D and 3D extensions of the DWP settings in BEC, which add one or two extra dimensions to the model, either without an additional potential, or with a periodic optical-lattice (OL) potential acting in these directions. These settings may be approximated, similar to the above-mentioned standard model of dual-core optical fibers, by a system of linearly coupled 1D [26] or 2D [27] equations. In a more accurate form, nearly 1D solitons can be found as solutions to the full 2D equation that includes the DWP (the potential depends on the transverse coordinate x, allowing solitons to self-trap in the free longitudinal direction y) [28]. The latter model is relevant to the case of the self-attractive nonlinearity. In the case of self-repulsion, dual-core gap solitons have been predicted in the setting with the OL potential applied along direction y [29]. Note that, in any setting, gap solitons cannot realize the ground state of the respective system, but, nevertheless, they represent stable configurations that have been created in the experiment using the condensate of ^{87}Rb atoms with the repulsion between them [30].

A general principle, upheld by the analysis in various settings (in nonlinear optics and BEC alike), is that the SSB occurs through bifurcations of symmetric or antisymmetric states, in the models with the self-attraction and self-repulsion, respectively. As mentioned above, models of the DWP or double-core type, combining cubic attractive and quintic repulsive nonlinearities, were studied too [13,14,31,32]. In the latter case, the competition between the self-focusing and self-defocusing against the backdrop of the DWP structure gives rise to specific SSB bifurcation diagrams, in the form of nonconvex closed loops [13,32], as well as to specific dynamical switching regimes [31]. Also predicted were manifestations of the SSB in a two-component BEC mixture trapped in the DWP structure [22], for both cases of the self-attraction and self-repulsion.

All the extensive work on the SSB outlined above was performed in settings based on usual linear potentials of the double-well type. The objective of the present work is to propose another physical framework, in which the SSB can be predicted in an effective *nonlinear* double-well potential (NDWP), induced through a spatial modulation of the local nonlinearity coefficient. Following the terminology commonly adopted in the solid-state theory [33], this nonlinear ingredient of the physical model may also be a called a *pseudopotential*.

In BEC settings, a pseudopotential structure may be readily induced through spatial modulation of the local value of the s-wave scattering length, $a_s(x)$, which determines the effective BEC nonlinearity. The modulation can be implemented, through the Feshbach resonance, by means of a spatially inhomogeneous dc magnetic field [34], or by a resonant optical field, as predicted in Ref. [35] and demonstrated experimentally in Ref. [36]. It was also proposed to control the Feshbach resonance by dint of dc electric field [37], which can be easily made inhomogeneous too. The attractive and repulsive interactions between atoms correspond to $a_s < 0$ and $a_s > 0$, respectively; both signs, as well as sign-changing patterns, can be used to engineer effective nonlinear potentials.

So designed pseudopotential lattices have attracted much interest in studies of BEC. In the 1D geometry, solitons, extended wave patterns, and various dynamical states supported by such structures were studied theoretically [38,39] (a random nonlinear lattice [40] and pseudopotentials generated by a spatially monotonous ramp of the local scattering length [41] were explored too). Recently, similar states were also considered in nonlinear optics, assuming a periodic modulation of the local Kerr coefficient [42]. Some (but much fewer) results were obtained too for 2D settings [43].

However, to the best of our knowledge, SSB phenomena in nonlinear pseudopotentials have not been studied yet. In this work, we focus on such effects in NDWP settings, which can be engineered by means of techniques mentioned above, using attractive interactions between atoms in BEC, or the self-focusing nonlinearity in optics, as briefly described below. In Sec. II, we formulate the model and give estimates of characteristic values of related physical parameters. Section III reports full analytical solutions corresponding to symmetric, antisymmetric, and *asymmetric* states trapped by the NDWP, in the limit case when the modulation of the local nonlinearity coefficient is represented by a set of two Dirac delta functions. The relevance of the latter model is stressed, in particular, by the recently introduced [39] BEC model with a periodic nonlinear potential of the Kronig-Penney type, whose simplest version reduces to a periodic array of delta functions (SSB effects were not studied in Ref. [39]).

In Sec. IV, we present numerical results for the general model, in which the delta functions are replaced by a pair of Gaussians of a finite width. In that case, the trapped states are found in a numerical form, and their stability is studied by means of direct simulations of slightly perturbed stationary states and also, independently, through the computation of respective stability eigenvalues for small perturbations. The result is that asymmetric states, which are unstable in the delta-function limit, can be readily stabilized in the general model. In addition, antisymmetric states may be stabilized also, in two disjoint regions of the parameter state, giving rise to a *bistability* involving antisymmetric and asymmetric states. A condition for the existence of symmetric states is that their norm must exceed a certain threshold value, in terms of their norm, an explanation to which is given. The existence and stability of all states, including a line of the SSB bifurcation, are summarized in a single diagram, which is presented in Sec. IV also. Results reported in this paper and perspectives for further work are summarized in Sec. V.

II. MODEL

The underlying 3D Gross-Pitaevskii equation for the mean-field wave function, $\Psi(X, Y, Z, T)$, is taken in the ordi-

nary form corresponding to the nearly 1D trap [44].

$$i\hbar\Psi_T = -\frac{\hbar^2}{2m}\nabla^2\Psi + \frac{m\omega_\perp^2}{2}R^2\Psi + \frac{4\pi\hbar^2 a_s(X)}{m}|\Psi|^2\Psi, \quad (1)$$

with m the atomic mass and $\omega_\perp$ the frequency providing for the tight confinement of the condensate in the direction of $R \equiv \sqrt{Y^2+Z^2}$. As said above, we assume an axial modulation (and negative sign) of the scattering length, in the form of a pair of Gaussians, each of width l and amplitude A_0, with centers set at points $X = \pm\Lambda$.

$$a_s(X) = -A_0\left[\exp\left(-\frac{(X+\Lambda)^2}{l^2}\right) + \exp\left(-\frac{(X-\Lambda)^2}{l^2}\right)\right]. \quad (2)$$

In what follows below, we measure the axial coordinate in units of Λ, and, accordingly, time in units of $m\Lambda^2/\hbar$, i.e., we define

$$x \equiv X/l, \quad a \equiv l/\Lambda, \quad t \equiv \hbar T/(m\Lambda^2). \quad (3)$$

Further, following the usual approach to the derivation of the effective 1D equation, we take the 3D field as a product of a slowly varying axial function, $\psi(X,T)$, and the ground-state wave function in the transverse plane,

$$\Psi = \frac{1}{\sqrt{2\pi^{5/2}aA_0\Lambda^2}}\exp\left(i\omega_\perp T - \frac{R^2}{2a_\perp^2}\right)\psi(x,t), \quad (4)$$

with $a_\perp^2 \equiv \hbar/(m\omega_\perp)$ [the scaling factor here is chosen so as to maintain normalization condition (7) (see below)].

The substitution of expression (4) in Eq. (1) and averaging in the transverse plane lead to the following 1D equation:

$$i\psi_t = -\frac{1}{2}\psi_{xx} + g(x)|\psi|^2\psi, \quad (5)$$

$$g(x) = -\frac{1}{a\sqrt{\pi}}\left[\exp\left(-\frac{(x+1)^2}{a^2}\right) + \exp\left(-\frac{(x-1)^2}{a^2}\right)\right], \quad (6)$$

where the modulated nonlinearity coefficient is subject to the following normalization condition:

$$\int_{-\infty}^{+\infty} g(x)dx \equiv 2. \quad (7)$$

Profiles of modulation function (6), which keeps the double-well structure for $a < \sqrt{2}$, are shown, for different values of a, in Fig. 1.

Equation (5) conserves two dynamical invariants, viz., the norm and energy (Hamiltonian),

$$N \equiv \int_{-\infty}^{+\infty}|\psi(x)|^2 dx, \quad H = \frac{1}{2}\int_{-\infty}^{\infty}(|\psi_x|^2 + g(x)|\psi|^4)dx. \quad (8)$$

As follows from Eqs. (4) and (3), the total number of atoms in the condensate, $\mathcal{N}$, is related to 1D norm N as follows:
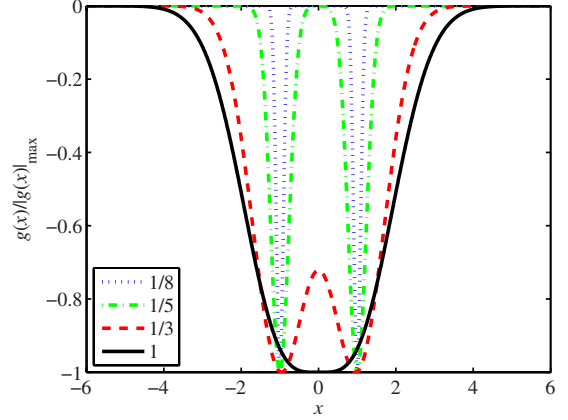

FIG. 1. (Color online) Shapes of double-well function (6), normalized to its maximum value, are shown for different values of scaled width a of the individual well.

$$\mathcal{N} \equiv \int\int\int|\Psi(X,Y,Z)|^2 dX dY dZ = \frac{a_\perp^2}{2\pi^{3/2}aA_0\Lambda}N. \quad (9)$$

For physical parameters relevant to experiments with the condensate of ^{7}Li atoms [45], i.e., $a_\perp \sim 2~\mu$m, $A_0 \sim 0.5$ nm, and $\Lambda \sim 20~\mu$m, characteristic values of the number of atoms in various patterns reported below [see, in particular, Figs. 3(d) and 9] fall into the range of $\mathcal{N}$ between $\sim$200 and 1000, which is quite sufficient for experimental manipulations and observation of the patterns. In the same range of physical parameters, $t=1$ in Eq. (5) is estimated as being tantamount to $\sim$10 ms, hence typical time scales for the instability development or intrinsic oscillations of breathers induced by the instabilities, which are reported below, are expected to be in the range of $0.1-1$ s, which is realistic to the currently available experimental techniques [45].

In terms of optical settings, a set of two narrow (of width $l \sim 1~\mu$m) parallel stripes with strong local nonlinearity can be built, in a planar waveguide, by means of known nano-technological methods. In that case, the power of the laser beam necessary for the self-trapping of transverse nonlinear patterns in the waveguide made of silica may be $\sim$500 kW [46], while using AlGaAs, one may reduce the necessary power to the level of 1 kW [47]. In these settings, the characteristic evolution length of the spatial beam can be made shorter than 1 mm. Obviously, transitions between states of different types reported in this paper may be relevant to the design of power-controlled optical-switching schemes. On the other hand, the description of the planar waveguide with the pair of embedded stripes may require a model more general than the one studied here, as it will plausibly combine the transverse modulation of the local nonlinearity with a similar linear potential (which is briefly described at the end of the next section), as the material difference between the stripes and host medium ought to affect the linear index of refraction also.

Stationary localized solutions to Eq. (5) are sought for as $\psi = e^{-i\mu t}\phi(x)$, where the chemical potential is negative, $\mu < 0$, and the real function $\phi(x)$ satisfies equation

$$\mu\phi + \frac{1}{2}\phi'' + \frac{1}{a\sqrt{\pi}}\left[\exp\left(-\frac{(x+1)^2}{a^2}\right) + \exp\left(-\frac{(x-1)^2}{a^2}\right)\right]\phi^3$$
$$= 0. \qquad (10)$$

An analytically solvable version of the model corresponds to the limit of $a \to 0$, with Eq. (5) going over into

$$i\psi_t = -(1/2)\psi_{xx} - [\delta(x+1) + \delta(x-1)]|\psi|^2\psi, \qquad (11)$$

where $\delta(x)$ is the Dirac's delta function. Note that rescaled equation (11) contains no free parameters; however, the norm of the solution will play the role of an intrinsic parameter (see below). In the same limit, stationary equation (10) takes the form of

$$\mu\phi + (1/2)\phi'' + [\delta(x+1) + \delta(x-1)]\phi^3 = 0. \qquad (12)$$

III. MODEL WITH THE DELTA FUNCTIONS: ANALYTICAL SOLUTIONS

A. Symmetric, antisymmetric, and asymmetric states

Off points $x = \pm 1$, Eq. (12) is linear. A general solution to this equation, decaying at $|x| \to \infty$, can be written as

$$\phi(x) = \begin{cases} B_1 e^{\sqrt{2|\mu|}(x+1)} & \text{at } x < -1 \\ A_0 e^{-\sqrt{2|\mu|}(x-1)} + B_0 e^{\sqrt{2|\mu|}(x+1)} & \text{at } -1 < x < +1 \\ A_1 e^{-\sqrt{2|\mu|}(x-1)} & \text{at } x > +1, \end{cases} \qquad (13)$$

with constant amplitudes A_0, A_1 and B_0, B_1. The continuity of the wave function at $x = \pm 1$ imposes two relations on them, $B_1 = B_0 + A_0 e^{2\sqrt{2|\mu|}}$, $A_1 = A_0 + B_0 e^{2\sqrt{2|\mu|}}$, which allows one to eliminate A_0 and B_0 in favor of A_1 and B_1,

$$A_0 = \frac{e^{2\sqrt{2|\mu|}}B_1 - A_1}{e^{4\sqrt{2|\mu|}} - 1}, \quad B_0 = \frac{e^{2\sqrt{2|\mu|}}A_1 - B_1}{e^{4\sqrt{2|\mu|}} - 1}. \qquad (14)$$

Further, the integration of Eq. (12) in infinitesimal vicinities of points $x = \pm 1$ yields expressions for jumps (Δ) of the first derivative at these points, $\Delta(\phi')|_{x=\pm 1} = -2(\phi|_{x=\pm 1})^3$. The substitution of solution (13) in these relations leads to a system of cubic equations for the amplitudes,

$$\sqrt{|\mu|/2}(B_1 - B_0 + A_0 e^{2\sqrt{2|\mu|}}) = B_1^3, \qquad (15)$$

$$\sqrt{|\mu|/2}(A_1 - A_0 + B_0 e^{2\sqrt{2|\mu|}}) = A_1^3. \qquad (16)$$

After the substitution of expressions (14) into Eqs. (16) and (15), we end up with two coupled cubic equations for A_1 and B_1 as follows:

$$\sqrt{2|\mu|}e^{2\sqrt{2|\mu|}}(e^{2\sqrt{2|\mu|}}B_1 - A_1) = (e^{4\sqrt{2|\mu|}} - 1)B_1^3, \qquad (17)$$

$$\sqrt{2|\mu|}e^{2\sqrt{2|\mu|}}(e^{2\sqrt{2|\mu|}}A_1 - B_1) = (e^{4\sqrt{2|\mu|}} - 1)A_1^3. \qquad (18)$$

Solving Eqs. (17) and (18), we first find symmetric and antisymmetric solutions,

$$A_1 = B_1 \equiv A_{\text{sym}} = \pm\sqrt{\frac{\sqrt{2|\mu|}}{1 + e^{-2\sqrt{2|\mu|}}}}. \qquad (19)$$

$$A_1 = -B_1 \equiv A_{\text{antisym}} = \pm\sqrt{\frac{\sqrt{2|\mu|}}{1 - e^{-2\sqrt{2|\mu|}}}}. \qquad (20)$$

The norm of these solutions, defined as per Eq. (8), is

$$N_{\text{sym,antisym}} = \frac{1}{1 \pm e^{-2\sqrt{2|\mu|}}} + \frac{1 - e^{-4\sqrt{2|\mu|}} \pm 4\sqrt{2|\mu|}e^{-2\sqrt{2|\mu|}}}{(1 \pm e^{-2\sqrt{2|\mu|}})^3}, \qquad (21)$$

with $+$ and $-$ corresponding to the symmetric and antisymmetric states, respectively. In the limit of $\mu \to -\infty$, both expressions (19) and (20) yield $A_{\text{sym}}^2(\mu = -\infty) = A_{\text{antisym}}^2(\mu = -\infty) = \sqrt{2|\mu|}$. In this limit, norm (21) of both solutions takes a common value, $N_{\text{sym,antisym}}(\mu = -\infty) = 2$. On the other hand, in the limit of $\mu \to -0$, the amplitude of the symmetric state vanishes, $A_{\text{sym}}(\mu \to -0) \approx (|\mu|/2)^{1/4}$, and its norm takes a finite limit value, $N_{\text{sym}}(\mu = 0) = 1/2$, while the amplitude of the antisymmetric state remains finite, $A_{\text{antisym}}(\mu \to -0) = 1/\sqrt{2}$, and its norm diverges, $N_{\text{antisym}}(\mu \to -0) \approx 1/(2\sqrt{2|\mu|})$. It can be easily checked that the decrease of N_{sym} and the increase of N_{antisym} with the variation of μ from $-\infty$ to 0 are not monotonous: N_{sym} attains a maximum, $(N_{\text{sym}})_{\text{max}} \approx 2.08$, at $\mu \approx -1.40$, and N_{antisym} has a minimum, $(N_{\text{antisym}})_{\text{min}} \approx 1.84$, at $\mu \approx -0.58$.

Actually, the finite minimum norm (*threshold*), necessary for the existence of the symmetric states, which is $N_{\text{sym}}(\mu = 0) \equiv (N_{\text{sym}})_{\text{min}} = 1/2$ in the present case, is a generic property, shared by the model with finite width a of the nonlinear-potential wells, as shown in detail below in Fig. 9. On the other hand, the existence of the above-mentioned maximum value of the norm for the symmetric states, $(N_{\text{sym}})_{\text{max}} \approx 2.08$, is a specific feature of the model with $a = 0$ (the one based on the delta functions): it is easy to see that, in the model with finite a, the norm of any state grows $\sim a\sqrt{|\mu|}$ at $\mu \to -\infty$. However, this specific feature, which, as a matter of fact, indicates degeneracy of the model with $a = 0$, is less significant for the physical applications, as all symmetric states, for $a = 0$ and finite a alike, are unstable when the norm exceeds its value at the SSB bifurcation point [further details can be seen in Eq. (23) and Fig. 9 below].

A point of the SSB bifurcation, which gives rise to a pair of asymmetric solutions splitting off from the symmetric one, can be easily found. Indeed, the symmetry breaking means that symmetric solution (19) acquires an infinitesimal *antisymmetric* addition, $\delta A_1 = -\delta B_1 \equiv \delta A$. Thus, infinitely close to the bifurcation point, the relevant solution is sought for as $A_1 = A_{\text{sym}} + \delta A$, $B_1 = A_{\text{sym}} - \delta A$. The substitution of this in Eqs. (17) and (18) and linearization in infinitesimal δA lead to a simple equation that predicts the value of the chemical potential at the bifurcation point: $\exp(\sqrt{2|\mu_{\text{bif}}|}) = \sqrt{2}$, or

$$\mu_{\text{bif}} = -(\ln 2)^2/8 \approx -0.06. \qquad (22)$$

At this point, the amplitude of symmetric solution (19) is $A_{\text{bif}} = \sqrt{(\ln 2)/3} \approx 0.481$, and the value of norm (8), with the upper sign, is
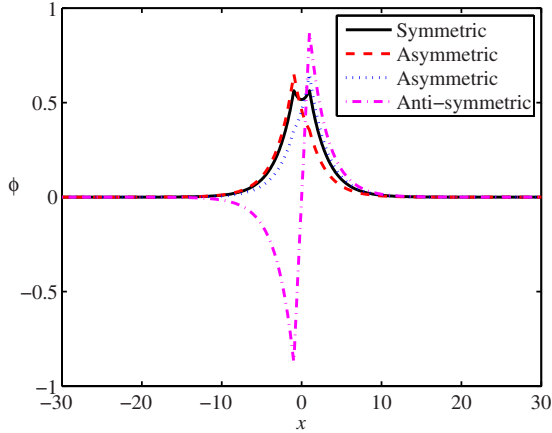
FIG. 2. (Color online) Profiles of symmetric, asymmetric, and antisymmetric stationary states in the analytically solvable model with the delta functions, all pertaining to $\mu = -0.1$. The respective values of the norm are $N_{\text{symm}} \approx 1.27$, $N_{\text{asymm}} \approx 1.07$, and $N_{\text{antisymm}} \approx 2.18$. The mutually symmetric lines (blue and red ones, in the color version of the figure) represent two asymmetric states that are mirror images of each other.

$$N_{\text{bif}} = 2/3 + (8/27)(3/4 + \ln 2) \approx 1.09. \qquad (23)$$

Actually, value (22) of the chemical potential at the bifurcation point is approximately the same in the model with finite-width nonlinear-potential wells, up to $a \approx 1$, as seen from Fig. 3(d) presented below.

The same analysis shows that antisymmetric solution (20) never gives rise to an antisymmetry-breaking bifurcation. Indeed, for this solution the antisymmetry would be broken by an infinitesimal symmetric variation, $\delta A_1 = \delta B_1 \equiv \delta A$, i.e., infinitely close to the bifurcation point, the solution would be $A_1 = A_{\text{antisym}} + \delta A$, $B_1 = -A_{\text{antisym}} + \delta A$. Subsequent substitution in Eqs. (17) and (18) and the linearization in δA yield an equation for μ that has no real solutions.

Equations (17) and (18) can be solved analytically for asymmetric states also:

$$\{A_1, B_1\}_{\text{asym}} = \frac{|\mu|^{1/4}(\sqrt{1 + 2e^{-2\sqrt{2|\mu|}}} \pm \sqrt{1 - 2e^{-2\sqrt{2|\mu|}}})}{2^{3/4}\sqrt{1 - e^{-4\sqrt{2|\mu|}}}}. \qquad (24)$$

Note that full solution (24) predicts exactly the same bifurcation point as Eq. (22), i.e., $\exp(\sqrt{2|\mu_{\text{bif}}|}) = \sqrt{2}$ [at this point, the second radical in Eq. (24) vanishes]. These solutions are characterized by the *asymmetry ratio*, which is defined as

$$\Theta = \frac{\displaystyle\int_0^{+\infty} \phi^2(x)dx - \int_{-\infty}^0 \phi^2(x)dx}{\displaystyle\int_{-\infty}^{+\infty} \phi^2(x)dx} \equiv \frac{N_+ - N_-}{N}. \qquad (25)$$

Typical examples of symmetric, asymmetric, and antisymmetric states produced by the above analytical solutions are displayed in Fig. 2.

B. Bifurcation diagrams and stability

The analytical solution given by Eqs. (13), (14), and (24) make it possible to plot the bifurcation diagrams in the planes of (μ, Θ) and (N, Θ), which are represented by curves pertaining to $a=0$ in Figs. 3(a)–3(c). To generate the diagrams, partial norms $N_\pm$ in expression (25) for the asymmetric solutions were computed numerically [analytical expressions for them are available, but they are very messy, cf. Eq. (21) for the symmetric and antisymmetric states].

A salient peculiarity of the SSB bifurcation for $a=0$, evident in Fig. 3(c), is its *subcritical* character, which means that the branches of asymmetric solutions emerge at the bifurcation point as unstable ones, and go in the *backward* direction. A subcritical bifurcation also occurs in the above-mentioned model of the dual-core nonlinear fibers [10], but in that case the asymmetric branches quickly turn in the forward direction, getting stabilized at the turning point. A remarkable feature of the present model with $a=0$ is that this does not happen, i.e., the bifurcation in this model may be called a "fully backward" one: the branches of the asymmetric solutions keep going backward up to the limit of $\Theta = 1$, which corresponds to the asymmetric solutions with $\mu = -\infty$ (and $N=1$, as shown in the following subsection). Indeed, $\Theta(\mu = -\infty) = 1$ follows from the fact that the amplitude appertaining to the lower sign between the radicals in Eq. (24) vanishes in the limit of $\mu \to -\infty$.

In accordance with general properties of the subcritical SSB bifurcation [10], the symmetric solution is expected to be stable below the bifurcation point [at $N < N_{\text{bif}}$, see Eq. (23)], and unstable above it. The asymmetric branches emerging at $N = N_{\text{bif}}$ are unstable as long as they go backward. In the present case ($a=0$), this means they are always unstable, as the respective branches in Figs. 3(b) and 3(c) never turn forward. All these expectations are completely borne out by the stability analysis performed by means of both direct simulations and computation of stability eigenvalues, at finite but small values of a (technical details of the procedure are described in the next section). In particular, at $N > N_{\text{bif}}$ the unstable symmetric state spontaneously transforms into a strongly asymmetric breather which features irregular oscillations, but remains robust as a whole (quite similar to an example displayed below in Fig. 6 for $a=0.7$). On the other hand, unstable asymmetric states transform themselves into breathers which maintain the original asymmetry of the unstable state, as shown in Fig. 4.

Lastly, all antisymmetric states in the model with delta functions are unstable too. Their instability is similar to that shown below in Fig. 7(b) for $a=1$, transforming them into strongly asymmetric breathers. As shown in the next section, both asymmetric and antisymmetric states may be stabilized in the general model, with finite a.

C. Concluding remarks concerning the delta-function model

The existence of the asymmetric states, i.e., the presence of the SSB effect in the present model, can be easily explained by the consideration of the above-mentioned limit of $\mu \to -\infty$. Indeed, in this limit, the spatial scale of the solution, which is $\sim |\mu|^{-1/2}$ according to Eq. (13), is much smaller than

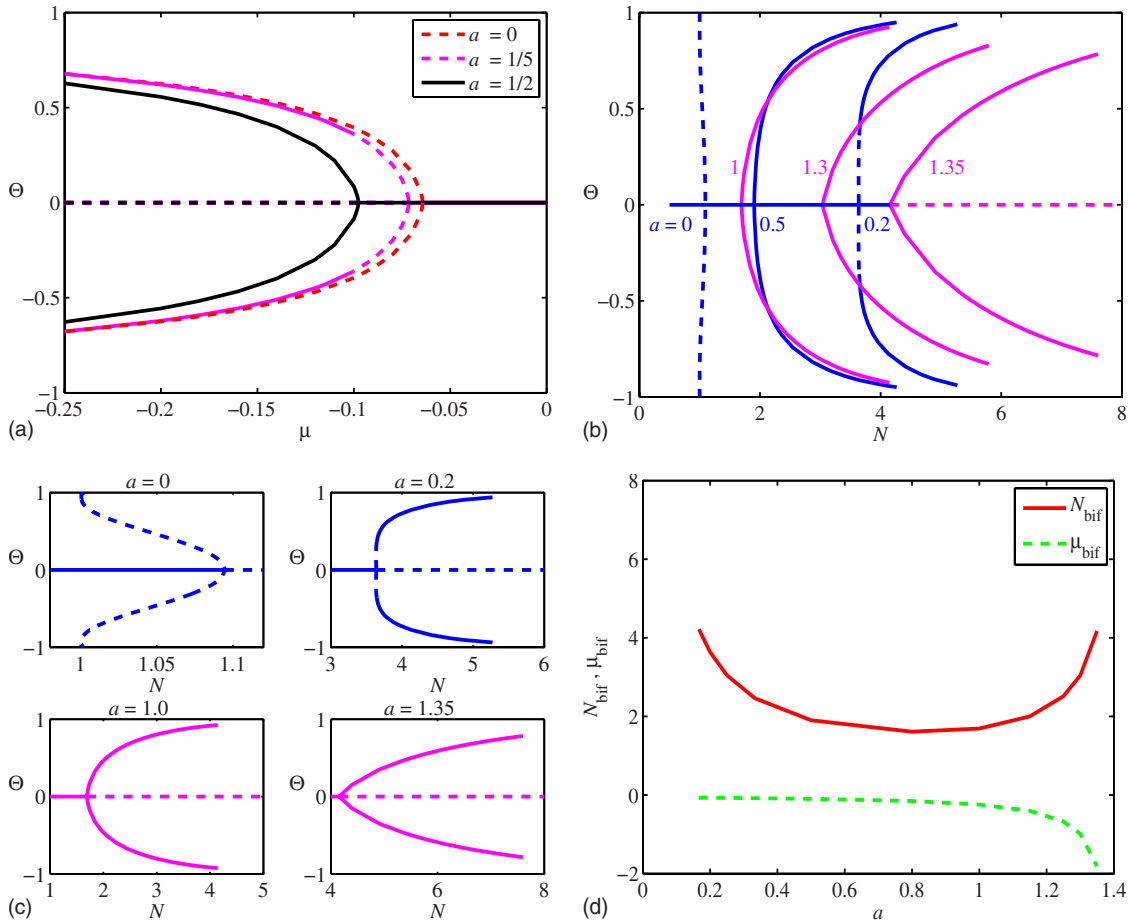FIG. 3. (Color online) Families of asymmetric states in the plane of (Θ, μ) (a) and (Θ, N) (b) for different fixed values of nonlinear-potential parameter a [recall that asymmetry ratio Θ is defined by Eq. (25), solution families with $\Theta \equiv 0$ being symmetric ones; panel (b) takes into regard the fact that symmetric states do not exist at $N < 1/2$]. Plots labeled "$a=0$" were generated by analytical solutions (13), (14), and (24). Panel (c) additionally displays solution branches from (b) near the bifurcation point, and (d) shows the coordinates of the bifurcation point, N_{bif} and μ_{bif}, as functions of a. Here and in Fig. 10 below, solid and dashed lines depict stable and unstable solutions, respectively. Note that the bifurcation observed in panels (b) and (c) at $a=0$ is a "fully backward" one: the branches of asymmetric states, which emerge at the bifurcation point, never turn forward and, accordingly, always remain unstable.

the separation between the two delta functions, $2\Lambda \equiv 2$. Therefore, the full solution effectively splits into a superposition of those independently supported by each delta function in isolation. Further, it is obvious that, for given large $|\mu|$, Eq. (12) with an individual delta function gives rise to two solutions: a trivial one, $\phi \equiv 0$, and

$$\phi_{\pm}(x) = \pm (2|\mu|)^{1/4} \exp(-\sqrt{2|\mu|}|\xi|), \quad (26)$$

where $\xi = x+1$ or $\xi = x-1$; note that the norm of solution (26) is $N=1$, for any μ. The corresponding symmetric and anti-symmetric states are built, respectively, as superpositions of solutions ϕ_+ (or, equivalently, ϕ_-) centered at $x=-1$ and $x=+1$, or ϕ_- centered at $x=-1$ and ϕ_+ centered at $x=+1$. Asymmetric solutions are represented, in the same limit, by a superposition of solution $\phi_{\pm}$ centered at $x=-1$ and zero solution around $x=+1$, or vice versa. Of course, finding the bifurcation point requires one to perform the analysis of the model at finite μ, as done in the analytical form above for the case of the delta functions, and will be done in a numerical form below for the general case of finite a in Eq. (6).

It is relevant to compare the above exact results with those which can be easily obtained in the linear counterpart of the model, i.e., the one with the DWP based on the set of two delta functions; as mentioned above, such a linear potential may be a plausible ingredient of a more general model, relevant to the description of NDWP settings in optics. The stationary version of the linear equation reduces to

$$\mu\phi + (1/2)\phi'' + \epsilon[\delta(x+1) + \delta(x-1)]\phi = 0, \quad (27)$$
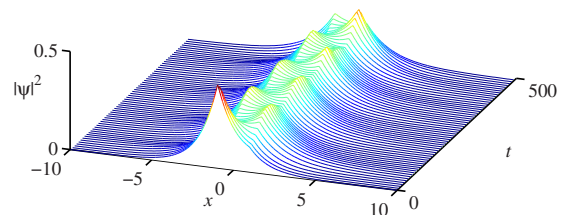

FIG. 4. (Color online) The evolution of an unstable asymmetric state for $a=1/60$ and $\mu=-0.1$.

with constant $\epsilon > 0$. Symmetric solutions, which must be continuous at $|x| = 1$, are sought for as

$$\phi(x) = \begin{cases} \exp[-\sqrt{2|\mu|}(|x| - 1)] & \text{at } |x| > 1 \\ \text{sech}(\sqrt{2|\mu|})\cosh(\sqrt{2|\mu|}x) & \text{at } |x| < 1, \end{cases} \quad (28)$$

cf. Eq. (13). The jump condition, $\Delta(\phi')|_{x=\pm 1} = -2\epsilon\phi(x = \pm 1)$, yields equation $\sqrt{2|\mu|}[1 + \tanh(\sqrt{2|\mu|})] = 2\epsilon$, which has a single solution for $|\mu|$ at any positive ϵ, i.e., the linear model always supports exactly one symmetric state.

Antisymmetric solutions are sought for as

$$\phi(x) = \begin{cases} \text{sgn}(x)\exp(-\sqrt{2|\mu|}(|x| - 1)) & \text{at } |x| > 1 \\ \text{cosech}(\sqrt{2|\mu|})\sinh(\sqrt{2|\mu|}x) & \text{at } |x| < 1, \end{cases}$$

and the respective jump condition takes the form of $\sqrt{2|\mu|}[1 + \coth(\sqrt{2|\mu|})] = 2\epsilon$. The latter equation has no solutions for $\epsilon < 1/2$, and exactly one solution for $\epsilon > 1/2$. Thus, symmetric solution (28) is the single state in the linear DWP model at $\epsilon < 1/2$, while at $\epsilon > 1/2$ the linear model supports precisely two states: symmetric and antisymmetric ones.

Lastly, the combined model, which includes both the linear potential and its nonlinear counterpart (that may be self-attractive, as above, or *self-repulsive* too, in this case), is also solvable in the case when these features are based on the pair of delta functions. The combined model is described by the following stationary equation, cf. Eqs. (12) and (27):

$$\mu\phi + (1/2)\phi'' + [\delta(x + 1) + \delta(x - 1)](\epsilon\phi + \sigma\phi^3) = 0, \quad (29)$$

where $\sigma = +1$ and -1 corresponds to the nonlinear attraction and repulsion, respectively. In particular, the bifurcation occurs only on the branch of the symmetric solutions in the case of $\sigma = +1$, and only on the antisymmetric branch—in the opposite case (self-repulsion). In either case, the value of the chemical potential ($\mu < 0$) at the symmetry- or antisymmetry-breaking bifurcation is determined by the following transcendental equation:

$$\sqrt{2|\mu|}\frac{1 - 2\sigma e^{-2\sqrt{2|\mu|}}}{1 - e^{-4\sqrt{2|\mu|}}} = \epsilon \quad (30)$$

[for $\epsilon = 0$ and $\sigma = +1$, it reduces to Eq. (22)]. With $\sigma = +1$, Eq. (30) has exactly one solution for any $\epsilon \geq -1/4$ and no solutions for $\epsilon < -1/4$ (negative ϵ corresponds to competition

between the repulsive linear potential and attractive nonlinear pseudopotential). With $\sigma = -1$, Eq. (30) has exactly one solution for any $\epsilon > 3/4$, and no solutions for $\epsilon < 3/4$. Analysis of the stability of states found in the combined model is beyond the scope of this work, and in the rest of the paper we consider the model without the linear potential.

IV. NUMERICAL RESULTS FOR THE GENERAL MODEL

A. Numerical methods

To construct localized solutions to stationary equation (10) of the symmetric, asymmetric, and antisymmetric types, the Newton iterative method was used, starting with the following inputs:

$$(\phi_0(x))_{\text{sym,asym}} = B\,\text{sech}(2(x + 1)) + A\,\text{sech}(2(x - 1)),$$

$$(\phi_0(x))_{\text{antisym}} = A\,\text{sech}(x)\sin(x),$$

with $B = A$ for symmetric solutions. Then, as mentioned above, numerical analysis of the stability of the stationary solutions was performed in two different ways: first, by means of direct simulations of the evolution of slightly perturbed solutions, and then through computation of (in)stability eigenvalues for modes of small perturbations. In the former case, the stability was tested by adding arbitrary perturbations to the initial state, at the level of $\sim 1\%$ of the amplitude (in particular, care was taken to test effects of perturbations whose symmetry is different from that of the stationary state, such as antisymmetric perturbations added to symmetric states, and vice versa).

For the computation of eigenvalues, perturbed solutions were looked for as

$$\psi(x,t) = e^{-i\mu t}\{\phi(x) + \eta[u(x)e^{i\lambda t} + v^*(x)e^{i\lambda^* t}]\}, \quad (31)$$

where $\phi(x)$ is a stationary solution to Eq. (10) with chemical potential μ, while u and v are components of a perturbation mode with an infinitesimal amplitude η, pertaining to instability growth rate $\lambda \equiv \lambda_r + i\lambda_i$. The substitution of expression (31) into Eq. (5) and linearization lead to the eigenvalue problem based on the following equations:

$$\begin{pmatrix} -\dfrac{1}{2}\dfrac{d^2}{dx^2} - \mu + 2g(x)\phi^2(x) & g(x)\phi^2(x) \\[2mm] -g(x)\phi^2(x) & +\dfrac{1}{2}\dfrac{d^2}{dx^2} + \mu - 2g(x)\phi^2(x) \end{pmatrix}\begin{pmatrix} u \\ v \end{pmatrix} = \lambda\begin{pmatrix} u \\ v \end{pmatrix}. \quad (32)$$

The underlying solution $\phi(x)$ is stable if all eigenvalues associated with it have $\lambda_i = 0$. Equations (32) were solved numerically with the help of a finite-difference method. Con-

clusions concerning the stability of the patterns, drawn from direct simulations, always complied with results produced by the computation of the eigenvalue.
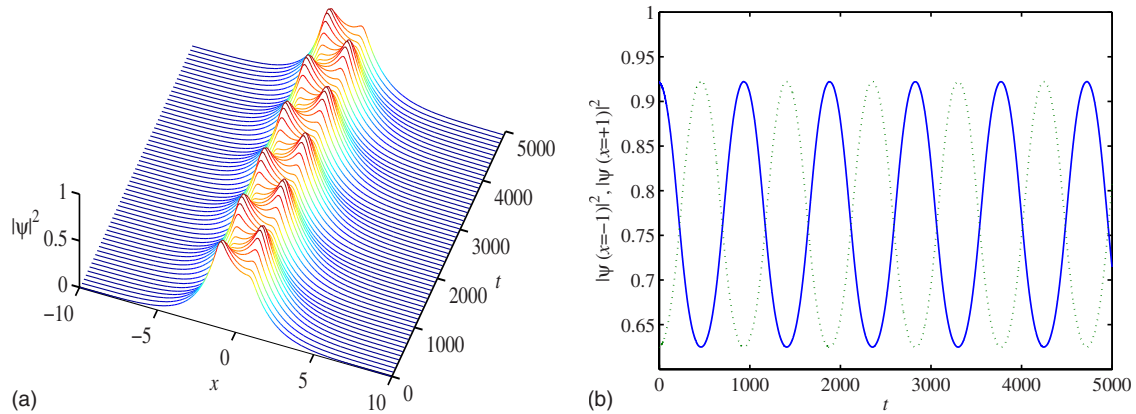
FIG. 5. (Color online) (a) The evolution of a weakly unstable asymmetric state with $a=0.2$ for $\mu=-0.075$ (very close to the bifurcation point and stabilization threshold). (b) For the same case, solid and dotted curves show densities $|\psi(x=-1)|^2$ and $|\psi(x=+1)|^2$ as functions of time.

B. Results

The first significant change against the results reported above for the model with the delta functions ($a=0$), which happens with the increase of a, is quick stabilization of asymmetric states with larger values of the norm, while ones with smaller N remain unstable, originally. At $a>0.2$, the symmetric states are stable for all values of N at which they exist. Another notable feature of the bifurcation diagrams at finite a, demonstrated by Figs. 3(b) and 3(d), is that the norm at which the SSB bifurcation takes place, N_{bif}, first decreases with the growth of a from small values up to $a\approx0.8$, and then increases with the further growth of a.

Close to their stabilization threshold (in particular, at $a=0.2$), asymmetric states with a smaller norm, which are still unstable, demonstrate a scenario of the instability development different from what was shown by their counterpart in Fig. 4 in the case of very small a. Namely, slow regular oscillations, observed in Fig. 5 in this case, imply a *dynamical resymmetrization* of the unstable asymmetric state. Indeed, densities $|\psi(x)|^2$, taken at points $x=\pm1$, perform identical periodic oscillations, with a phase shift of π between them, as shown in Fig. 5(b).

The stabilization of the asymmetric states at small finite values of a is explained by the change in the character of the SSB bifurcation: at $a\neq0$, there appear turning points on branches of asymmetric solutions in the bifurcation diagram, cf. Fig. 3(c). Past the turning point, the branch goes forward as a *stable* one. In fact, Fig. 3(c) demonstrates a quick transformation, with the increase of a, of the subcritical bifurcation into a supercritical one. When the bifurcation is supercritical, branches of the asymmetric solutions emerge as stable ones at the bifurcation point, and immediately go forward.

We do not display the quick transition from the sub-to supercritical bifurcation in full detail, as it actually happens at very small a, in the range of $a\lesssim0.1$. The physical estimates given in Sec. II suggest that so small values of the scaled width of the nonlinear-potential wells correspond to physical widths $\lesssim1$ μm. It seems doubtful that the Feshbach-resonance technique would allow one to create a strong local inhomogeneity of the scattering length on such a

small scale (nevertheless, the exact analytical solutions obtained for $a=0$, which provide clear clues for the understanding of the general model, are definitely relevant). An additional problem impeding the full analysis of the case of very small a is that, in this case, the accumulation of systematic numerical results requires very heavy simulations, as the step size of the spatial grid must be made much smaller than a.

Above the bifurcation point, symmetric states found at finite a demonstrate the familiar SSB instability, spontaneously transforming themselves into slightly nonstationary robust modes (breathers), quite close in their shape to respective stable asymmetric solitons. A typical example of this transformation is displayed in Fig. 6.

As concerns antisymmetric solutions, both stable and unstable ones have been found at finite a, as illustrated by Figs. 7 and 8. Figure 7(b) shows that the density profile of unstable antisymmetric states evolves from the double-peak pattern into an asymmetric single-peak one, which features persistent intrinsic oscillations. This outcome of the instability development complies with the fact that the instability of the antisymmetric states is oscillatory, being accounted for by a quartet of eigenvalues, as seen in Fig. 8(b). In other words, the transition from stable to unstable antisymmetric states may be considered as the *Hamiltonian Hopf bifurcation* [48].

Figure 9 displays a combined diagram in the plane of the norm of the solution and width of the nonlinear potential wells, N and a, which summarizes the existence and stability results for the states of all three types—symmetric, asymmetric, and antisymmetric ones. The dashed-dotted line in the
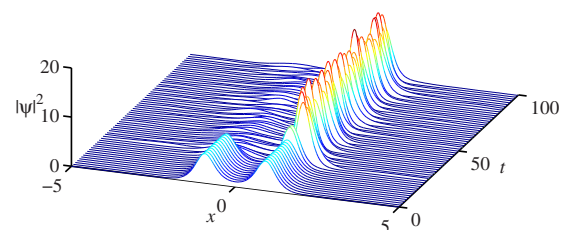

FIG. 6. (Color online) The evolution of an unstable symmetric state, at $a=0.7$, $\mu=-2.677$, and $N=10$.
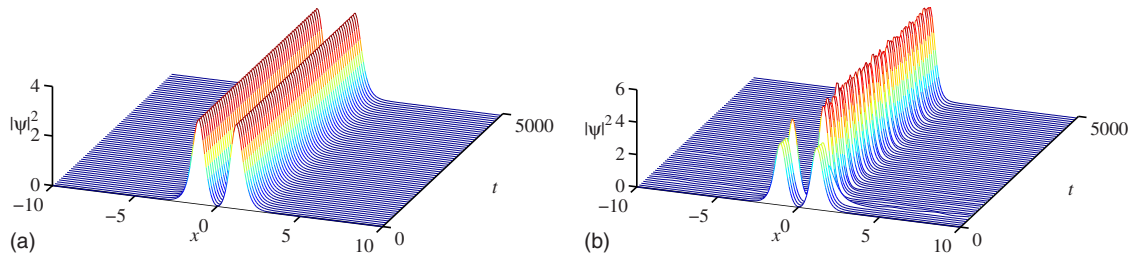
FIG. 7. (Color online) (a) An example of a stable antisymmetric state with $a=1$, for $\mu=-1.3$ and $N=6.7137$. (b) The evolution of an unstable antisymmetric state, also with $a=1$, but for $\mu=-1.5$ and $N=7.1273$.

figure designates the symmetry-breaking bifurcation. Solely symmetric states exist below this line (they are stable in that region), and stable asymmetric states exist above the line, where the symmetric ones are unstable. Solid curves in Fig. 9 depict stability borders of antisymmetric solutions.

For the reasons explained above, the region of very small values of a, where the "quick" stabilization of asymmetric states takes place, is not included. However, the region of the existence of the analytical symmetric and antisymmetric solutions in the model with delta functions ($a=0$), and the respective bifurcation point, as given by Eq. (23), are shown by the bold vertical segment and square-marked dot on the axis of $a=0$ (recall that the exact asymmetric solutions are unstable above the bifurcation point in the model with $a=0$).

Because the modulation profile (6) does not feature the double-well structure for $a \geq \sqrt{2}$ (see Fig. 1), the SSB bifurcation tends to disappear as a approaches $\sqrt{2}$. Actual results are included in Fig. 9 for $a \lesssim 1.35$, as the convergence of the numerical scheme becomes poor for values of a still closer to $\sqrt{2}$.

The chain of circles in Fig. 9 designates the threshold (minimum norm) N_{min}, necessary for the existence of symmetric states in the model. As mentioned above, in the case of $a=0$ the exact threshold is $N_{min}(a=0)=1/2$, and it is observed in Fig. 9 that the threshold remains in the ballpark of this value at finite a, which can be easily explained. Indeed, the minimum of N is attained at $\mu \rightarrow -0$, in which limit the spatial scale of the wave function, $\sim 1/\sqrt{2|\mu|}$, is much larger than the size of the NDWP structure, $2\Lambda \equiv 2$. Thus, from the viewpoint of this weakly localized wave function, modulation pattern (6) looks like $2\delta(x)$. In the corresponding approximation, the wave function takes the form of expression (26) divided by $\sqrt{2}$, and the respective norm is, indeed, $1/2$.

For $N < N_{min}$, the condensate confined to the trap of large length L (i.e., in the thermodynamic limit) will tend to form a quasiuniform nearly linear state, with $\phi(x)=\sqrt{N/L}$. As follows from Eqs. (8) and (6), the energy of the small-amplitude uniform state is

$$H_0 \approx -N^2/L^4. \tag{33}$$

In fact, this state realizes a minimum of the energy (cf. Fig. 10), i.e., the system's ground state. Nevertheless, a well-known fact is that dynamically stable localized states *different* from the ground state, such as the above-mentioned gap solitons in the repulsive condensate [30], or their broader counterparts in the form of the so-called gap waves [49], can be created in the experiment.

Another notable feature observed in Fig. 9 is the *bistability*, i.e., the coexistence of stable asymmetric and antisymmetric states above the stability border of the latter state. In fact, the bistability always takes place when antisymmetric states are stable. It is interesting too that the stability area for the antisymmetric states consists of two separate regions. Finally, it is relevant to mention that, as well as in the analytically solvable model with the delta functions ($a \rightarrow 0$), the antisymmetric states never undergo a bifurcation at finite a.

We stress that the stability borders displayed in Fig. 9 were identified by means of direct simulations and the computation of stability eigenvalues, both methods yielding identical results. In particular, the sets of eigenvalues displayed in Fig. 8 clearly confirm the presence of two disjoint stability areas for antisymmetric states.

In the case of the bistability involving the asymmetric and antisymmetric states, it is interesting to compare their energies (values of the Hamiltonian). To this end, Fig. 10 displays a typical example of the dependence of H on norm N. The situation observed in this figure is also true in the general case: stable antisymmetric states realize smaller values of H than the asymmetric counterparts coexisting with them. However, as argued above, dynamically stable states can be created in the experiment even if their energy is higher than in some competing states. In particular, Fig. 6 demonstrates that an unstable symmetric state definitely self-traps into an asymmetric robust breather (which is close to a stable stationary solution), despite the fact that a stable antisymmetric
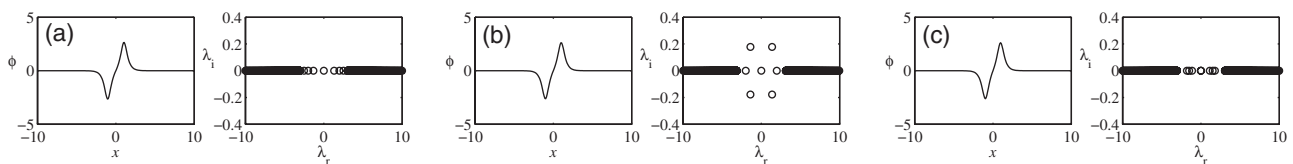

FIG. 8. Examples of stable [(a) and (c)] and unstable [(b)] antisymmetric states, found with a fixed norm, $N=10$. In each subplot, the left and right panels show profiles of the stationary states and spectral planes of the (in)stability eigenvalues. Parameters are (a) $a=0.80$ and $\mu=-3.05$; (b) $a=1.11$ and $\mu=-3.14$; (c) $a=1.30$ and $\mu=-3.07$.
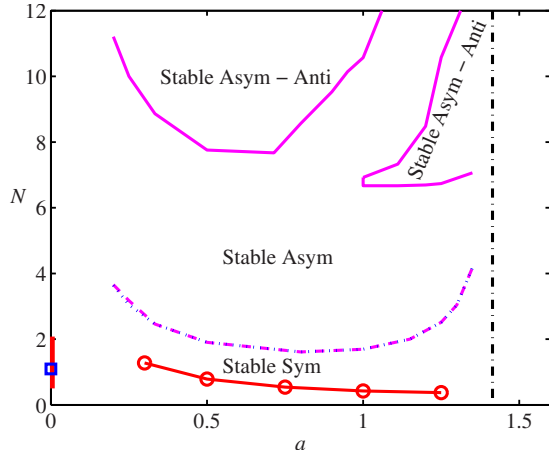
FIG. 9. (Color online) Stability and existence borders for symmetric, asymmetric, and antisymmetric states in the plane of (a, N). The vertical dashed-dotted line corresponds to $a = \sqrt{2}$, beyond which the double-well structure in Eq. (6) turns into a single-well one. The lower dashed-dotted line depicts the symmetry-breaking bifurcation, with stable asymmetric solutions existing above it. The chain of circles in the bottom of the parameter plane designates the minimum norm necessary for the existence of symmetric states, which are stable between the existence border and the bifurcation line. Label "Stable Asym- -Anti" marks regions of the bistability, where both asymmetric and antisymmetric states are stable.

FIG. 10. (Color online) The Hamiltonian versus the norm for solutions of different types, with fixed $a = 0.75$.

state exists at the same values of $N = 10$ and $a = 0.7$, as seen from Fig. 9.

Note that all curves in Fig. 10 start from finite threshold values of N corresponding, as said above, to the minimum norm $(N_{\min})$ necessary for the existence of the respective states. In particular, for the branch of symmetric solutions, $N_{\min}$ is close to $1/2$, as argued above (cf. the existence border in the bottom of Fig. 9), while the asymmetric branch originates at the bifurcation point (in agreement with the location of the respective dashed-dotted line in Fig. 9), at which the symmetric solution loses its stability. The branch of antisymmetric solutions features a fold in Fig. 10 (in the region where these solutions are unstable), which is similar to the above-mentioned fact that dependence $N(\mu)$ in Eq. (21) for the unstable exact antisymmetric states has a minimum, $(N_{\mathrm{antisym}})_{\min} \approx 1.84$ at $\mu \approx -0.58$. If replotted in terms of H and N, Eq. (21) features a similar fold, at $N = (N_{\mathrm{antisym}})_{\min}$.

V. CONCLUSION

In this work, we have introduced a model of the NDWP, alias a double-well pseudopotential, which can be created in BEC, by means of the spatially inhomogeneous Feshbach resonance, and also in nonlinear optics. The model provides for a previoulsy unexplored setting in which effects of the SSB can be studied.

In the limit when each potential well is induced by the delta function, full analytical solutions were obtained for symmetric, antisymmetric, and asymmetric states. The symmetric states are stable in that case up to the symmetry-
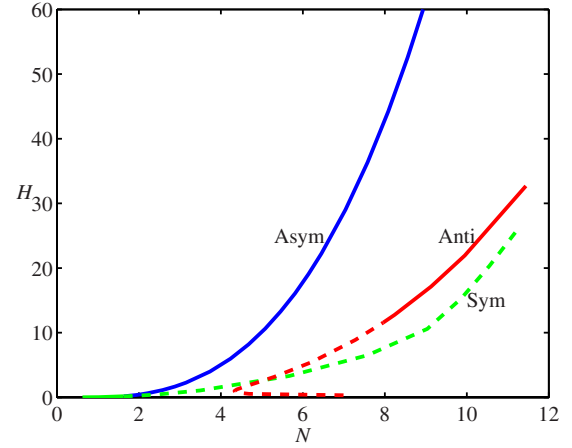
breaking bifurcation point, but beyond the bifurcation both symmetric and emergent asymmetric states are unstable. In particular, the asymmetric configurations transform themselves into breathers. The instability of all the stationary asymmetric states in the model with the delta functions is explained by the fact that the respective SSB bifurcation is of a "fully backward" type, with branches of the asymmetric solutions never turning forward. All antisymmetric states are unstable too, in this limit form of the model.

The increase of the width of the potential wells readily stabilizes the asymmetric states, which concurs with the change of the character of the SSB bifurcation from sub- to supercritical. Close to the stabilization border, unstable asymmetric states develop slow intrinsic oscillations, featuring effective dynamical resymmetrization. Antisymmetric states may also be stable in the NDWP structure with a finite width of the wells, which implies the bistability between asymmetric and antisymmetric states. The symmetric states exist above a finite threshold, in terms of the norm (number of atoms in the condensate), and they develop the usual SSB instability above the bifurcation point. A simple explanation to the existence threshold was given, and an integrated diagram for the existence and stability of the trapped states of all three types has been produced.

The analysis presented in this work suggests new experiments in the matter-wave and nonlinear-optical settings. The analysis can also be developed in other directions. In particular, it may be interesting to study a two-dimensional nonlinear-DWP configuration. In the 2D space, a triangular configuration with three nonlinear (pseudo-)potential wells may be considered too.

[1] K. Hayata and M. Koshiba, J. Opt. Soc. Am. B **9**, 1362 (1992).

[2] C. Cambournac, T. Sylvestre, H. Maillotte, B. Vanderlinden, P. Kockaert, Ph. Emplit, and M. Haelterman, Phys. Rev. Lett. **89**, 083901 (2002).

[3] P. G. Kevrekidis, Z. Chen, B. A. Malomed, D. J. Frantzeskakis, and M. I. Weinstein, Phys. Lett. A **340**, 275 (2005).

[4] B. Maes, M. Soljacic, J. D. Joannopoulos, P. Bienstman, R. Baets, S.-P. Gorza, and M. Haelterman, Opt. Express **14**, 10678 (2006).

[5] M. Ornigotti, G. D. Valle, D. Gatti, and S. Longhi, Phys. Rev. A **76**, 023833 (2007).

[6] B. V. Gisin, A. Kaplan, and B. A. Malomed, Phys. Rev. E **62**, 2804 (2000).

[7] S. M. Jensen, IEEE J. Quantum Electron. **18**, 1580 (1982); A. M. Maier, Kvantovaya Elektron. (Moscow) **9**, 2296 (1982); [Sov. J. Quantum Electron. **12**, 1490 (1982)].

[8] D. D. Gusovskii, E. M. Dianov, A. A. Maier, V. B. Nestruev, V. V. Osiko, A. M. Prokhorov, K. Yu. Sitarskii, and I. A. Shcherbakov, Sov. J. Quantum Electron. **17**, 724 (1987); S. Trillo, S. Wabnitz, E. M. Wright, and G. I. Stegeman, Opt. Lett. **13**, 672 (1988); S. R. Friberg, A. M. Weiner, Y. Silberberg, B. G. Sfez, and P. S. Smith, *ibid.* **13**, 904 (1988).

[9] A. W. Snyder, D. J. Mitchell, L. Poladian, D. R. Rowland, and Y. Chen, J. Opt. Soc. Am. B **8**, 2102 (1991).

[10] F. Kh. Abdullaev, R. M. Abrarov, and S. A. Darmanyan, Opt. Lett. **14**, 131 (1989); E. M. Wright, G. I. Stegeman, and S. Wabnitz, Phys. Rev. A **40**, 4455 (1989); C. Paré and M. Florjanczyk, *ibid.* **41**, 6287 (1990); N. Akhmediev and A. Ankiewicz, Phys. Rev. Lett. **70**, 2395 (1993); P. L. Chu, B. A. Malomed, and G. D. Peng, J. Opt. Soc. Am. B **10**, 1379 (1993); J. M. Soto-Crespo and N. Akhmediev, Phys. Rev. E **48**, 4710 (1993); B. A. Malomed, I. M. Skinner, P. L. Chu, and G. D. Peng, *ibid.* **53**, 4084 (1996).

[11] W. C. K. Mak, P. L. Chu, and B. A. Malomed, J. Opt. Soc. Am. B **15**, 1685 (1998); Y. J. Tsofe and B. A. Malomed, Phys. Rev. E **75**, 056603 (2007).

[12] W. C. K. Mak, B. A. Malomed, and P. L. Chu, Phys. Rev. E **55**, 6134 (1997).

[13] L. Albuch and B. A. Malomed, Math. Comput. Simul. **74**, 312 (2007).

[14] A. Sigler and B. A. Malomed, Physica D **212**, 305 (2005).

[15] N. N. Akhmediev and A. V. Buryak, J. Opt. Soc. Am. B **11**, 804 (1994).

[16] A. Gubeskys and B. A. Malomed, Eur. Phys. J. D **28**, 283 (2004).

[17] A. Sigler, B. A. Malomed, and D. V. Skryabin, Phys. Rev. E **74**, 066604 (2006).

[18] B. D. Esry and C. H. Greene, Phys. Rev. A **59**, 1457 (1999).

[19] L. E. Sadler, J. M. Higbie, S. R. Leslie, M. Vengalattore, and D. M. Stamper-Kurn, Nature (London) **443**, 312 (2006).

[20] M. Albiez, R. Gati, J. Fölling, S. Hunsmann, M. Cristiani, and M. K. Oberthaler, Phys. Rev. Lett. **95**, 010402 (2005).

[21] S. Raghavan, A. Smerzi, S. Fantoni, and S. R. Shenoy, Phys. Rev. A **59**, 620 (1999); E. A. Ostrovskaya, Y. S. Kivshar, M. Lisak, B. Hall, F. Cattani, and D. Anderson, *ibid.* **61**, 031601(R) (2000); T. Kapitula and P. G. Kevrekidis, Nonlinearity **18**, 2491 (2005); D. Ananikian and T. Bergeman, Phys. Rev. A **73**, 013604 (2006); G. Theocharis, P. G. Kevrekidis, D. J. Frantzeskakis, and P. Schmelcher, Phys. Rev. E **74**, 056608 (2006).

[22] C. Wang, P. G. Kevrekidis, N. Whitaker, and B. A. Malomed, e-print arXiv:0805.0023, Physica D (to be published).

[23] K. W. Mahmud, J. N. Kutz, and W. P. Reinhardt, Phys. Rev. A **66**, 063607 (2002); P. Ziń, E. Infeld, M. Matuszewski, G. Rowlands, and M. Trippenbach, Phys. Rev. A **73**, 022105 (2006).

[24] S. Raghavan, A. Smerzi, and V. M. Kenkre, Phys. Rev. A **60**, R1787 (1999); A. Smerzi and S. Raghavan, *ibid.* **61**, 063601 (2000); D. R. Dounas-Frazer, A. M. Hermundstad, and L. D. Carr, Phys. Rev. Lett. **99**, 200402 (2007).

[25] G. Watanabe and C. J. Pethick, Phys. Rev. A **76**, 021605(R) (2007).

[26] A. Gubeskys and B. A. Malomed, Phys. Rev. A **75**, 063602 (2007).

[27] A. Gubeskys and B. A. Malomed, Phys. Rev. A **76**, 043623 (2007).

[28] M. Matuszewski, B. A. Malomed, and M. Trippenbach, Phys. Rev. A **75**, 063621 (2007).

[29] M. Trippenbach, E. Infeld, J. Gocałek, M. Matuszewski, M. Oberthaler, and B. A. Malomed, Phys. Rev. A **78**, 013603 (2008).

[30] B. Eiermann, Th. Anker, M. Albiez, M. Taglieber, P. Treutlein, K.-P. Marzlin, and M. K. Oberthaler, Phys. Rev. Lett. **92**, 230401 (2004).

[31] R. Driben, B. A. Malomed, and P. L. Chu, J. Phys. B **39**, 2455 (2006).

[32] Z. Birnbaum and B. A. Malomed, e-print arXiv:0802.0667, Physica D (to be published).

[33] W. A. Harrison, *Pseudopotentials in the Theory of Metals* (Benjamin, New York, 1966).

[34] S. Inouye, M. R. Andrews, J. Stenger, H. J. Miesner, D. M. Stamper-Kurn, and W. Ketterle, Nature (London) **392**, 151 (1998); Ph. Courteille, R. S. Freeland, D. J. Heinzen, F. A. van Abeelen, and B. J. Verhaar, Phys. Rev. Lett. **81**, 69 (1998); J. L. Roberts, N. R. Claussen, J. P. Burke, C. H. Greene, E. A. Cornell, and C. E. Wieman, *ibid.* **81**, 5109 (1998).

[35] P. O. Fedichev, Yu. Kagan, G. V. Shlyapnikov, and J. T. M. Walraven, Phys. Rev. Lett. **77**, 2913 (1996).

[36] M. Theis, G. Thalhammer, K. Winkler, M. Hellwig, G. Ruff, R. Grimm, and J. H. Denschlag, Phys. Rev. Lett. **93**, 123001 (2004).

[37] M. Marinescu and L. You, Phys. Rev. Lett. **81**, 4596 (1998).

[38] H. Sakaguchi and B. A. Malomed, Phys. Rev. E **72**, 046610 (2005); G. Fibich, Y. Sivan, and M. I. Weinstein, Physica D **217**, 31 (2006); J. Garnier and F. K. Abdullaev, Phys. Rev. A **74**, 013604 (2006); D. L. Machacek, E. A. Foreman, Q. E. Hoq, P. G. Kevrekidis, A. Saxena, D. J. Frantzeskakis, and A. R. Bishop, Phys. Rev. E **74**, 036602 (2006); M. A. Porter, P. G. Kevrekidis, B. A. Malomed, and D. J. Frantzeskakis, Physica D **229**, 104 (2007); J. Belmonte-Beitia, V. M. Pérez-García, V. Vekslerchik, and P. J. Torres, Phys. Rev. Lett. **98**, 064102 (2007); F. Abdullaev, A. Abdumalikov, and R. Galimzyanov, Phys. Lett. A **367**, 149 (2007); G. Dong and B. Hu, Phys. Rev. A **75**, 013625 (2007); D. A. Zezyulin, G. L. Alfimov, V. V. Konotop, and V. M. Pérez-García, *ibid.* **76**, 013621 (2007); Z. Rapti, P. G. Kevrekidis, V. V. Konotop, and C. K. R. T. Jones, J. Phys. A: Math. Theor. **40**, 14151 (2007); H. A. Cruz, V. A. Brazhnyi, and V. V. Konotop, J. Phys. B **41**, 035304 (2008); L. C. Qian, M. L. Wall, S. L. Zhang, Z. W. Zhou, and H. Pu, Phys. Rev. A **77**, 013611 (2008); F. K. Ab-

dullaev, A. Gammal, M. Salerno, and L. Tomio, *ibid.* **77**, 023615 (2008).

[39] A. S. Rodrigues, P. G. Kevrekidis, M. A. Porter, D. J. Frantzeskakis, P. Schmelcher, and A. R. Bishop, Phys. Rev. A **78**, 013611 (2008).

[40] F. K. Abdullaev and J. Garnier, Phys. Rev. A **72**, 061605(R) (2005).

[41] G. Theocharis, P. Schmelcher, P. G. Kevrekidis, and D. J. Frantzeskakis, Phys. Rev. A **72**, 033614 (2005); M. I. Rodas-Verde, H. Michinel, and V. M. Pérez-García, Phys. Rev. Lett. **95**, 153903 (2005).

[42] R. Y. Hao, R. C. Yang, L. Li, and G. S. Zhou, Opt. Commun. **281**, 1256 (2008).

[43] H. Sakaguchi and B. A. Malomed, Phys. Rev. E **73**, 026601 (2006); G. Dong, B. Hu, and W. Lu, Phys. Rev. A **74**, 063601 (2006); R. Y. Hao and G. S. Zhou, Chin. Opt. Lett. **6**, 211

(2008).

[44] C. J. Pethick and H. Smith, *Bose-Einstein Condensation in Dilute Gases* (Cambridge University Press, London, 2002).

[45] K. E. Strecker, G. B. Partridge, A. G. Truscott, and R. G. Hulet, New J. Phys. **5**, 73 (2003).

[46] J. S. Aitchison, Y. Silberberg, A. M. Weiner, D. E. Leaird, M. K. Oliver, J. L. Jackel, E. M. Vogel, and P. W. E. Smith, J. Opt. Soc. Am. B **8**, 1290 (1991).

[47] F. Lederer, G. I. Stegeman, D. N. Christodoulides, G. Assanto, M. Segev, and Y. Silberberg, Phys. Rep. **463**, 1 (2008).

[48] J.-C. van der Meer, Nonlinearity **3**, 1041 (1990); P. D. Woods and A. R. Champneys, Physica D **129**, 147 (1999).

[49] Th. Anker, M. Albiez, R. Gati, S. Hunsmann, B. Eiermann, A. Trombettoni, and M. K. Oberthaler, Phys. Rev. Lett. **94**, 020403 (2005).